International Journal of Modern Physics C
Vol. 21, No. 2 (2010) 261–274
© World Scientific Publishing Company
DOI: 10.1142/S0129183110015105

World Scientific
www.worldscientific.com

LATTICE BOLTZMANN SIMULATION OF ELECTROOSMOTIC MICROMIXING BY HETEROGENEOUS SURFACE CHARGE

G. H. TANG*, F. F. WANG and W. Q. TAO
State Key Laboratory of Multiphase Flow
School of Energy and Power Engineering
Xi'an Jiaotong University, Xi'an 710049, China
* *ghtang@mail.xjtu.edu.cn*

Received 28 October 2009
Accepted 10 December 2009

Microelectroosmotic flow is usually restricted to low Reynolds number regime, and mixing in these microfluidic systems becomes problematic due to the negligible inertial effects. To gain an improved understanding of mixing enhancement in microchannels patterned with heterogeneous surface charge, the lattice Boltzmann method has been employed to obtain the electric potential distribution in the electrolyte, the flow field, and the species concentration distribution, respectively. The simulation results show that heterogeneous surfaces can significantly disturb the streamlines leading to apparently substantial improvements in mixing. However, the introduction of such a feature can reduce the mass flow rate in the channel. The reduction in flow rate effectively prolongs the available mixing time when the flow passes through the channel and the observed mixing enhancement by heterogeneous surfaces partly results from longer mixing time.

Keywords: Lattice Boltzmann method; electroosmotic flow; mixing; microchannel.

1. Introduction

Recent developments in microfabrication technologies have enabled a variety of miniaturized fluidic systems consisting of microducts, valves, pumps, nozzles, and others. However, microfluidic devices are not simply scale-down version of conventional ones because fluid behavior at microscale and macroscale are quite different. To optimize design and operation, a better understanding of microscale fluidic transport phenomena is essential, e.g. surface effects such as molecular interactions and electrokinetic effects become important.

Because of no moving component, electroosmotic flow (EOF) is often a very preferred pumping method for microdevices. Bulk flow in a microchannel can be achieved by applying an external electric field along the channel. However, EOF is usually operated in a low Reynolds number regime so that efficient mixing becomes a problem due to negligible inertial effect. Species mixing in electroosmotic flow is inherently diffusion dominated, requiring either a long mixing channel or sufficient residence time to achieve a homogeneous solution. To enhance mixing, one

approach is to use mechanical methods such as microstirrers. However, in addition to the fabrication cost, these methods with moving components are not reliable for practical applications.

Generally, one of the common approaches with no moving parts for enhancing mixing in electroosmotic flow is using heterogeneous zeta potential on the surfaces.[1–9] To ensure an optimal device design and operation, we need quantitative understanding on how such a feature enhances species mixing. This study will focus on the mixing enhancement method by patterning heterogeneous surface charge on microchannel walls and discuss both the mixing efficiency and mixing time. The new insight could help microdevice optimal design and operation which were largely by trial-and-error before.

2. Numerical Methods

The recent development of the lattice Boltzmann (LB) method has provided an alternative simulation tool for computational fluid dynamics. As a derivative of lattice gas automata (LGA), the LB method differs from traditional numerical methods which solve the conventional macroscopic governing equations for the conserved fields such as flow field. The LB method tracks the evolution of the distribution functions of the microscopic particles to describe the conserved fields. This provides a method for obtaining streaming patterns in complicated systems. Recently, LB model has also successfully been used in modeling a range of microfluidics electroosmosis applications.[9–15] Here, in addition to describing flow field, LB method will be used to model electric potential distribution and species concentration field. One benefit of such an approach is the ease of programing because the computations for the electric potential, the velocity field, and the species concentration field, are all within the same framework. This feature could especially be more useful for a multiprocessor code in parallel computing.

The rest of the paper is organized as follows. In Sec. 2, we present the discrete Boltzmann equations for the velocity fields, the electric potential and the concentration fields. Section 3 presents numerical simulations of electroosmotic flow in uniform channels and channels patterned with heterogeneous surfaces. A brief conclusion is given in Sec. 4.

2.1. *The discrete lattice Boltzmann equation*

The discrete lattice Boltzmann equation with the Bhatnagar–Gross–Krook (BGK) collision approximation, including an external force term, can be written as a general form[16]

$$f_i(\mathbf{r} + \mathbf{c}_i\delta_t, t + \delta_t) = f_i(\mathbf{r}, t) - \frac{\delta_t}{\tau}[f_i(\mathbf{r}, t) - f_i^{\mathrm{eq}}(\mathbf{r}, t)] + A\,, \tag{1}$$

where f is the distribution function, τ is the relaxation time, $\mathbf{c}_i$ is the particle discrete velocity, δ_t is the lattice timestep, and A is a substitution term representing the external force. For a D2Q9 square lattice, the discrete particle velocities

can be written as $\mathbf{c}_0 = 0$ (the zero velocity distribution), $\mathbf{c}_i = (\cos[(i-1)\pi/2], \sin[(i-1)\pi/2])c$ for $i = 1, 2, 3, 4$ and $\mathbf{c}_i = (\cos[(i-5)\pi/2+\pi/4]), \sin[(i-5)\pi/2+\pi/4])\sqrt{2}c$ for $i = 5, 6, 7, 8$, where $c = \delta_x/\delta_t$ is the particle streaming speed satisfying $c = \sqrt{3RT}$ and δ_x is the lattice spacing step.

In Eq. (1), $f_i^{\mathrm{eq}}(i = 0, 1, \ldots, 8)$ is the equilibrium density distribution. For a D2Q9 lattice it can be represented by a general form

$$f_i^{\mathrm{eq}} = \omega_i B\,, \tag{2}$$

where B is a substitution parameter and the weighting coefficient $\omega_0 = 4/9$, $\omega_i = 1/9$ for $i = 1, 2, 3, 4$ and $\omega_i = 1/36$ for $i = 5, 6, 7, 8$. Within the same LB framework, we just need to adjust the substitution term A in Eq. (1) and substitution parameter B in Eq. (2) for electric potential, velocity, and concentration in sequence during the simulations. Note that f_i independently represents the distribution function of the electric potential, velocity, and concentration accordingly.

2.1.1. *The electric potential*

From the electrostatic theory, the electric potential can be described by the Poisson equation:

$$\nabla^2\Phi = -\frac{\rho_e}{\varepsilon\varepsilon_0}\,, \tag{3}$$

where ρ_e is the electric charge density, ε_0 is the permittivity of free space and ε is the relative dielectric constant of the solution. Generally, the electric potential, Φ, can be decomposed into a potential due to the external electric field, ϕ, and a potential due to the electric double layer (EDL), ψ, i.e. $\Phi = \phi + \psi$.[17] Therefore, Eq. (3) can be rewritten as[17]

$$\nabla^2\phi = 0\,, \tag{4}$$

and

$$\nabla^2\psi = -\frac{\rho_e}{\varepsilon\varepsilon_0}\,. \tag{5}$$

During this study, we employ a uniform $\nabla\phi$ along the streamwise direction in the simulated smooth channels instead of solving Eq. (4). Assuming that the equilibrium Boltzmann distribution is applicable, the net charge density distribution can be expressed as the sum of all the ions in the solution[17]:

$$\rho_e = \sum_\alpha z_\alpha e n_{\alpha,\mathrm{inf}} \exp\left(-\frac{z_\alpha e\psi}{k_{\mathrm{B}}T}\right)\,, \tag{6}$$

where z_α and $n_{\alpha,\mathrm{inf}}$ are the valence and the bulk ionic concentration of type α ions, respectively. The bulk ionic concentration, n_{inf} is the product of the ionic molar concentration, c_{inf} and Avogadro's number, N_A. The constant e is the charge of a

proton, and k_{B} is Boltzmann's constant. Substituting Eq. (6) into Eq. (5) yields the nonlinear Poisson–Boltzmann equation:

$$\nabla^2\psi + \frac{1}{\varepsilon\varepsilon_0}\sum_{\alpha} z_\alpha e n_{\alpha,\mathrm{inf}} \exp\left(-\frac{z_\alpha e\psi}{k_{\mathrm{B}}T}\right) = 0\,. \tag{7}$$

Assuming a uniform dielectric constant and neglecting any fluctuations in the dielectric constant (since the ion-convection effect is insignificant compared to ion diffusion when the Peclet number is less than one hundred[18]), we can write the net charge density distribution in a symmetric electrolyte, which is proportional to the concentration difference between the cations and anions, as[19]

$$n_{\pm} = n_{\mathrm{inf}} \exp\left(\mp\frac{ze\psi}{k_{\mathrm{B}}T}\right)\,, \tag{8}$$

$$\rho_e = ze(n_+ - n_-) = -2zen_{\mathrm{inf}} \sinh\left(\frac{ze\psi}{k_{\mathrm{B}}T}\right)\,. \tag{9}$$

If assuming Eq. (7) as the steady state of an original second-order partial equation in terms of ψ including temporal derivative, we can similarly obtain the substitution term A in the LB Eq. (1) for the evolution of the electric potential due to the EDL

$$A = \delta_t\left(\frac{1}{\varepsilon\varepsilon_0}\sum_{\alpha} z_\alpha e n_{\alpha,\mathrm{inf}} \exp\left(-\frac{z_\alpha e\psi}{k_{\mathrm{B}}T}\right)\right)\omega_i\,, \tag{10}$$

and the substitution parameter $B = \psi$. The potential diffusivity, χ, which is equal to unity in the simulations, is related to the relaxation time by

$$\chi = \frac{\tau - 0.5\delta_t}{3}\frac{\delta_x^2}{\delta_t^2}\,. \tag{11}$$

The macroscopic electric potential in the liquid is obtained from

$$\psi = \sum_i f_i\,. \tag{12}$$

2.1.2. *The flow field*

For the flow field, we have the substitution term

$$A = \delta_t\frac{\mathbf{F}\cdot(\mathbf{c}_i - \mathbf{u})}{RT} f_i^{\mathrm{eq}}(\mathbf{r}, t)\,, \tag{13}$$

where $\mathbf{u}$ is the macroscopic velocity, T is the temperature, R is the gas constant, and $\mathbf{F}$ is the external force acting per unit mass, and[20]

$$B = \rho\left[1 + \frac{3(\mathbf{c}_i\cdot\mathbf{u})}{c^2} + \frac{9(\mathbf{c}_i\cdot\mathbf{u})^2}{2c^4} - \frac{3(\mathbf{u}\cdot\mathbf{u})}{2c^2}\right]\,. \tag{14}$$

The mass density and momentum density can be obtained by summing over the distribution function, $f_i(\mathbf{r}, t)$ like

$$\rho = \sum_i f_i \quad \text{and} \quad \rho\mathbf{u} = \sum_i f_i \mathbf{c}_i \,. \tag{15}$$

The kinematic viscosity, ν, is given by

$$\nu = \frac{\tau - 0.5\delta_t}{3} \frac{\delta_x^2}{\delta_t^2} \,. \tag{16}$$

Using the Chapman–Enskog approximation, it can be shown that Eq. (1) recovers the momentum conservation expression in the Navier–Stokes equations:

$$\rho \left(\frac{\partial \mathbf{u}}{\partial t} + (\mathbf{u} \cdot \nabla)\mathbf{u} \right) = -\nabla p + \rho\nu\nabla^2\mathbf{u} + \rho\mathbf{F} \,, \tag{17}$$

where p is the pressure and $\rho\mathbf{F}$ is the electrical force acting on the fluid, relating to the electric potential Φ by $\rho\mathbf{F} = -\rho_e \nabla\Phi$.

2.1.3. *The species concentration field*

In general, a species is transported by convection of the carrier fluid and diffusion due to the concentration gradient. By applying the lattice Boltzmann method to describe the species transport in the solute, we have $A = 0$ and

$$B = c_d \left[1 + \frac{3(\mathbf{c}_i \cdot \mathbf{u})}{c^2} + \frac{9(\mathbf{c}_i \cdot \mathbf{u})^2}{2c^4} - \frac{3(\mathbf{u} \cdot \mathbf{u})}{2c^2} \right] . \tag{18}$$

The species concentration c_d is obtained by

$$c_d = \sum_i f_i \,. \tag{19}$$

Again, applying the Chapman–Enskog expansion, it can be shown that the LB equation for species transport recovers the normal continuum equation for convection and diffusion[21]:

$$\frac{\partial c_d}{\partial t} + (\mathbf{u} \cdot \nabla) c_d = D\nabla^2 c_d \,, \tag{20}$$

where the diffusion coefficient, D, is related to the corresponding relaxation time via

$$D = \frac{\tau - 0.5\delta_t}{3} \frac{\delta_x^2}{\delta_t^2} \,. \tag{21}$$

Note that the LB equations with the general form of Eq. (1) for electric potential distribution in the electrolyte, the flow field, and the species concentration are not coupled together and the equations are solved in sequence during the present study. The parameters of δ_t, c, and τ are adjusted independently in different cases.

2.2. *Boundary conditions*

The lattice Boltzmann method becomes an ideal simulation tool for fluid flows in complex geometries because the boundary conditions can readily be implemented. To solve the LB equation for the electric potential, the zeta potentials on the upper and lower walls are fixed and Dirichlet boundary conditions are employed.[22] Periodic boundary conditions are employed for the electric potential at the channel inlet and outlet. For the velocity field, we have adopted the non-slip boundary condition[23] on the upper and lower walls and used periodic boundary condition at the inlet and outlet. At the channel inlet where the sample meets buffer, the sample is injected at the upper half of the channel while the buffer moves in at the lower half of channel. Therefore, the species concentration is unity across the upper half of the channel and zero across the lower half of the channel. A first-order extrapolation is adopted for the inlet boundary whilst Neumann boundary conditions (with $\partial c_d/\partial \mathbf{n} = 0$) are implemented along the solid walls, so that species cannot penetrate into the wall. Extrapolation scheme is again used at the outlet to determine the unknown concentration distributions.

3. Results and Discussion

3.1. *Electroosmotic mixing in uniform microchannels*

First, a simple electroosmotic flow between two parallel plates is considered. The upper and lower surfaces are defined by $y = H$ and $y = 0$, respectively, the channel height is set to be $H = 10$ μm and the channel length $L = 10H$. The simulated channel serves as a representative component of an integrated chip and both H and L are flexible design parameters that can easily be adjusted. Unless otherwise specified, $\varepsilon\varepsilon_0 = 7.79 \times 10^{-10}$ C^2/(J $\cdot$ m), $T = 293$ K, $e = 1.6 \times 10^{-19}$ C, $N_A = 6.02 \times 10^{23}$ mol^{-1}, $k_{\mathrm{B}} = 1.38 \times 10^{-23}$ J/K, $\rho = 998.2$ kg/m^3, $z = +1$, $\nu = 1.004 \times 10^{-6}$ m^2/s, the uniform zeta potential of $\zeta = -100$ mV on the whole surface. External DC electrodes are located at the two ends of the channel and the externally-applied electric field between the channel inlet and outlet is fixed at $\Delta\phi = 5$ V, which sustains a uniform externally-applied electric intensity of $\nabla\phi = -500$ V/cm in the present simulation.

Figure 1 presents the species concentration distribution across the channel at uniformly spaced cross-sections along the channel ($X = x/L$) for $c_{\mathrm{inf}} = 10^{-5}$ mol/l and $D = 10^{-10}$ m^2/s. As the mixing proceeds from the channel inlet ($c_d = 0$ for $0 \le Y \le 0.5$, and $c_d = 1$ for $0.5 < Y \le 1$) to the outlet, the concentration difference between the upper and lower streams becomes smaller. Since the mixing process is dominated by diffusion, the channel length is insufficient to have a homogeneously mixed sample at the outlet. To obtain a fully-mixed solution ($c_d = 0.5$), a longer residence time is needed to allow the species to mix. This can be achieved by either extending the channel length or by applying a smaller electric field.

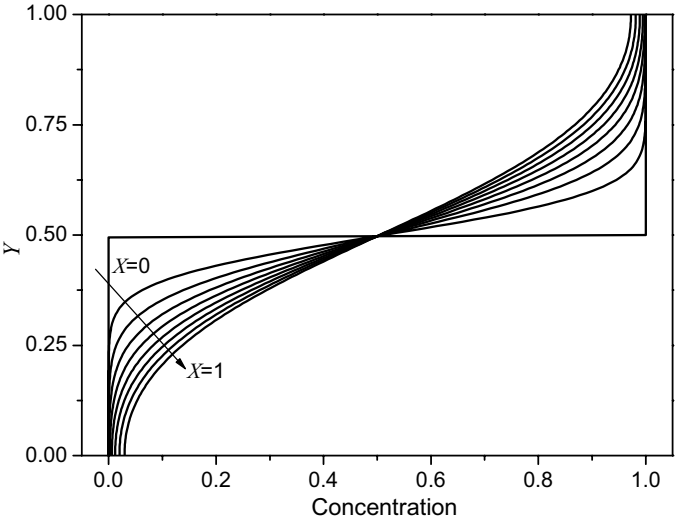

Fig. 1. Species concentration profiles from the channel inlet ($X = 0$) to the outlet ($X = 1$) for $c_{\text{inf}} = 10^{-5}$ mol/l and $D = 10^{-10}$ m^2/s.

To quantify the mixing enhancement at the channel cross-sections along the streamwise direction, a mixing efficiency can be calculated from[7]:

$$\sigma(x) = \left(1 - \frac{\int_0^H |c_d - c_{d,\text{inf}}| dy}{\int_0^H |c_{d,0} - c_{d,\text{inf}}| dy}\right) \times 100\% \,, \tag{22}$$

where $c_{d,0}$ and $c_{d,\text{inf}}$ are the species concentrations in the completely unmixed ($c_{d,0} = 0$ or 1) and completely mixed ($c_{d,\text{inf}} = 0.5$) states, respectively. The calculated mixing efficiency from the channel inlet to the outlet is presented in Fig. 2(a) for different diffusion coefficients and bulk ionic concentrations. As the mixing proceeds, the gradients of the mixing efficiency curves diminish due to the decreasing concentration difference between the upper and lower flow streams. The figure clearly shows that the current operating conditions are only suitable for species that have a large diffusion coefficient. To mix a species having a smaller diffusion coefficient, it would be necessary to use a lower electric field gradient to ensure sufficient mixing time.

Previous studies have usually focused only on the mixing efficiency since this is one of the most important parameters when comparing the effectiveness of different mixing enhancement methods. However, the mixing efficiency cannot be considered in isolation since the mixing time is also an important parameter in the design of a real device. We cannot afford a mixing enhancement method with unnecessary long mixing time. In the present study, we analyze the mixing process in terms of the mixing time, $t(x)$, for the species to travel from the inlet to position, x, along the channel. The total mixing time is the time required for a species to pass from the entrance to the exit of the microchannel. A desirable mixing enhancement method

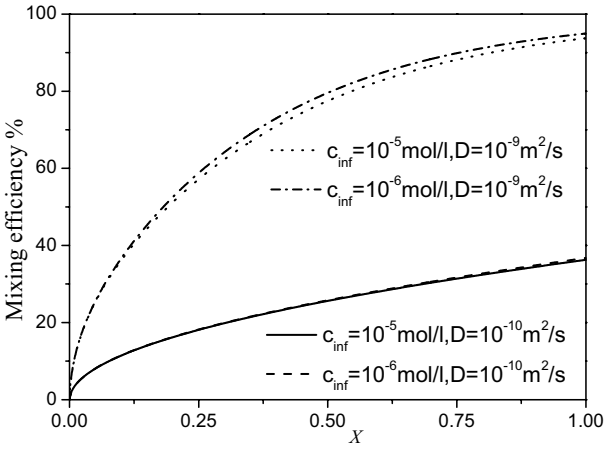

(a)

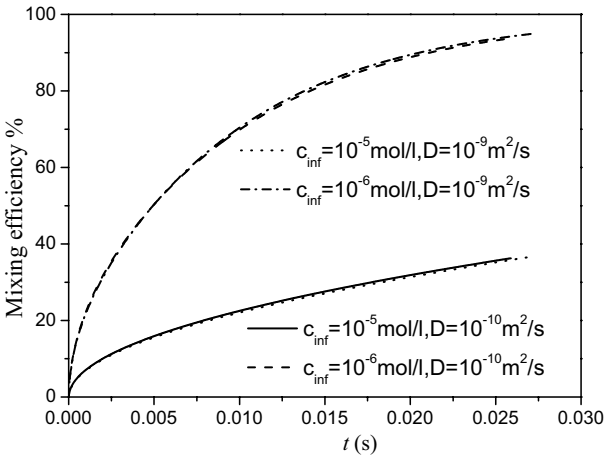

(b)

Fig. 2. Species mixing efficiency profiles from the channel inlet to the outlet. (a) Mixing efficiency against distance. (b) Mixing efficiency against mixing time.

must achieve a good mixing efficiency without significant reduction of overall flow rate.

Figure 2(b) presents the mixing efficiency against the mixing time $t(x)$. Although the average velocity for $c_{\inf} = 10^{-5}$ mol/l is larger than that for $c_{\inf} = 10^{-6}$ mol/l, it can be seen that the same species achieves very similar mixing efficiencies for different bulk ionic concentrations. Figure 2(b) indicates that there are small variations in the mixing efficiency profile which are due to differences in the velocity magnitude and shear rate. For $D = 10^{-9}$ m^2/s, the samples are nearly fully mixed at the end of the channel and can achieve about 80% mixing within the first 0.015 s.

However, for $D = 10^{-10}$ m^2/s, the operating conditions are not optimized for mixing, and it would be necessary to reduce the flow rate by adjusting the applied electric field. In addition, it can be seen that the mixing profiles against time are very similar for the same diffusion coefficient implying that it is mainly the mixing time that causes the different mixing efficiencies seen in Fig. 2(a). The prolonged mixing time will increase the molecular diffusion process and thereby improves the mixing efficiency at a certain location.

3.2. *Electroosmotic flow in heterogeneous microchannels*

To achieve a completely homogeneous solution in a relatively short channel, especially for a species with a relatively low diffusion coefficient, high mixing performance is essential. We consider the effect of introducing a heterogeneous zeta potential along the surface of the channel. This is a commonly adopted approach for enhancing the mixing in electroosmotic flows[1–8] and can be achieved by fabricating the surface from different materials or by modifying the local surface charge e.g. using electrodes buried beneath the substrate or through laser ablation. In practice, it is also possible to obtain variations in the zeta potential due to contamination of the microchannel walls, variations in the wall coating, or gradients in the buffer pH.[24]

The ionic molar concentration is fixed at $c_{\text{inf}} = 10^{-5}$ mol/l and the diffusion coefficient $D = 10^{-10}$ m^2/s in the following sections, which is a general value for commonly used chemical reagents.

The test problem consists of a smooth channel with six heterogeneous patches of $\zeta_w = +100$ mV applied along $X = 0.2$–0.25, 0.4–0.45, and 0.6–0.65 on the bottom wall, $X = 0.3$–0.35, 0.5–0.55, and 0.7–0.75 on the top wall, while the other surfaces of the channel are maintained at a uniform zeta potential of $\zeta = -100$ mV. Figure 3

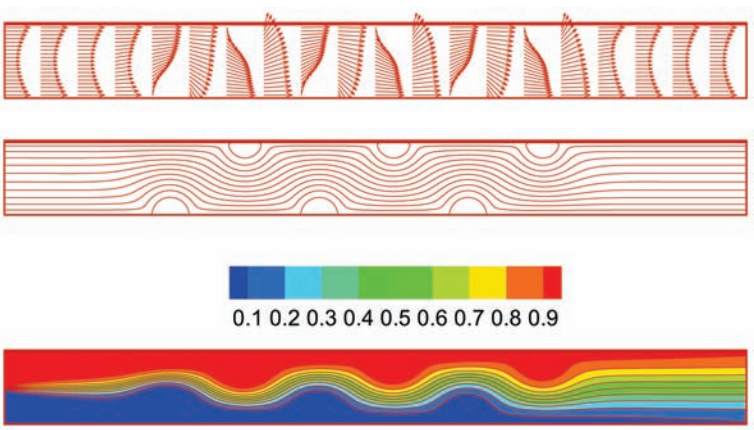

Fig. 3. (Color online) Velocity vectors, streamlines and species concentration contours in a microchannel composed of six sections of heterogeneous surface (from the top to the bottom).

presents the velocity vectors, streamlines and species concentration distribution for the case with six sections of heterogeneous surface. We can clearly see the presence of flow disturbances in the heterogeneous regions. The velocity vectors indicate that the fluid undergoes a change in flow direction and the streamlines show local recirculation zones in the vicinity of the heterogeneous patches. In addition, the velocity profiles away from the heterogeneous regions exhibit a significant "concave" flow distribution.

Figure 4(a) shows the mixing efficiency with two ($X = 0.2$–0.25 on the bottom wall, and $X = 0.3$–0.35 on the top wall), four ($X = 0.2$–0.25 and $X = 0.4$–0.45 on

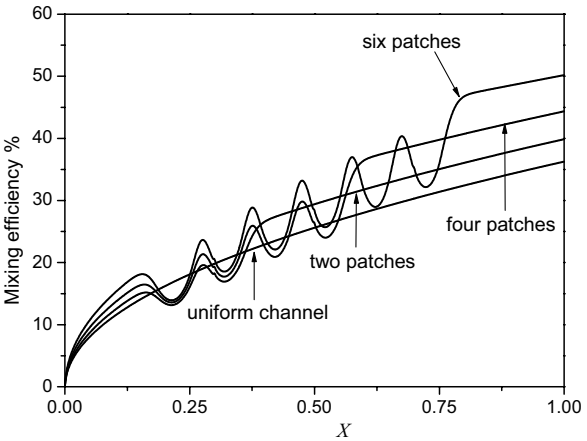

(a)

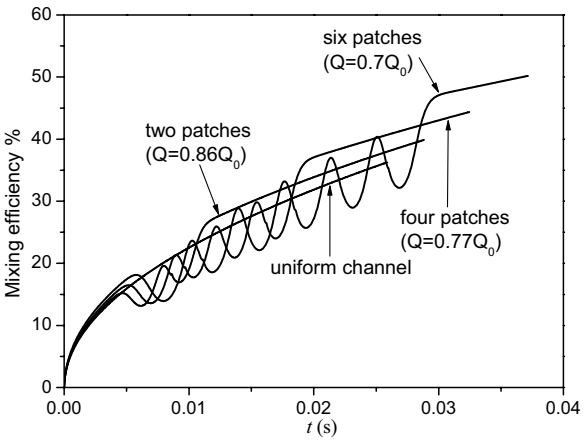

(b)

Fig. 4. Species mixing efficiency of the uniform and heterogeneous channels showing the effect of different numbers of heterogeneous patch. (a) Mixing efficiency against distance. (b) Mixing efficiency against mixing time. Q is the mass flow rate and Q_0 is the mass flow rate for the uniform surface potential channel.

the bottom wall, and $X = 0.3$–0.35 and $X = 0.5$–0.55 on the top wall), and six heterogeneous patches, in comparison with a uniform channel surface potential of $\zeta = -100$ mV. The mixing efficiency at the channel outlet is 39.9, 44.4, and 50.2% for two patches, four patches, and six patches, respectively. It can be seen that the introduction of a heterogeneous surface enhances the mixing, especially for multiple heterogeneous sections. However, Fig. 4(b) demonstrates that the enhancement in the mixing efficiency is partly caused by the increased total mixing time due to the decreased flow rate. In Fig. 4(b), the mass flow rate per unit width for the smooth channel is $Q_0 = 2.32 \times 10^{-5}$ kg/s. The corresponding calculated mean velocity across the channel is 0.00386 m/s, which is in good agreement with the Helmholtz–Smoluchouski electroosmotic velocity in the standard electroosmotic flow, $u_{\mathrm{HS}} = 0.00389$ m/s, calculated by[25]

$$u_{\mathrm{HS}} = \frac{\varepsilon\varepsilon_0\zeta}{\mu}\nabla\phi\,, \tag{23}$$

where μ is the fluid dynamic viscosity. Note that the mass flow rate is reduced by introducing heterogeneous zeta potential on the microchannel surface. Consequently, there is more time available for species to mix.

It is informative to consider the effect of changing the zeta potential of the heterogeneous patch whilst keeping the surface potential of the remaining walls fixed at $\zeta = -100$ mV. Figure 5 indicates that the recirculation zones only occur when the heterogeneous surface potential is of the opposite sign ($\zeta_w = +150$ mV) to that of the homogeneous surface ($\zeta = -100$ mV). In addition, the size of the recirculation zone is observed to increase as the magnitude of the heterogeneous potential increases. The presence of a large recirculating eddy causes the bulk flow to be forced away from the heterogeneous patch and pass through a narrower region increasing the local concentration gradients which enhance the mixing. The streamwise velocity near the heterogeneous patch is slightly increased for the case of $\zeta_w = -150$ mV, while it is slightly decreased for the case of $\zeta_w = -50$ mV. For both cases in which the heterogeneous surface potential is of the same sign to that of the homogeneous surface, the streamlines only exhibit slightly tortuous approaching and departing the heterogeneous patch regions.

Figure 6(a) shows the mixing efficiency for different values of zeta potential on the six heterogeneous patches ($\zeta_w = -150$, -50, $+100$ and $+150$ mV). It can be seen that the mixing efficiency increases when the magnitude of the heterogeneous

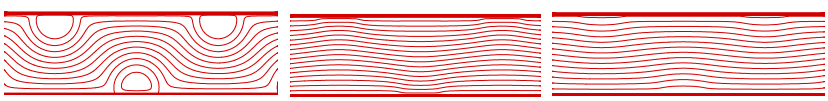

(a) (b) (c)

Fig. 5. (Color online) Detail of the streamlines in the vicinity of the heterogeneous patch. (a) $\zeta_w = +150$ mV. (b) $\zeta_w = -150$ mV. (c) $\zeta_w = -50$ mV.

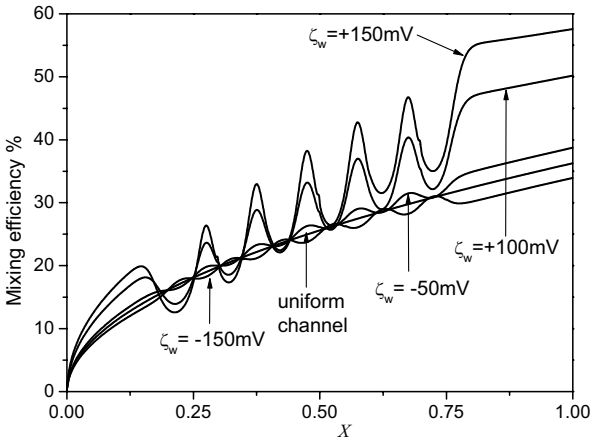

(a)

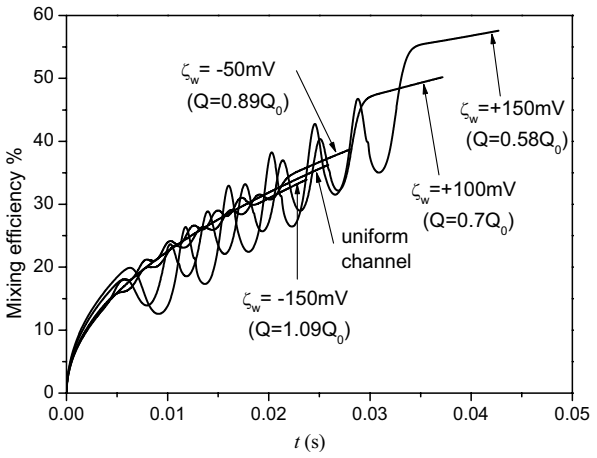

(b)

Fig. 6. Species mixing efficiency of the uniform and heterogeneous channels. (a) Mixing efficiency against distance. (b) Mixing efficiency against mixing time. Q is the mass flow rate and Q_0 is the mass flow rate for the uniform surface potential channel.

potential of opposite sign increases, and decreases when the heterogeneous potential of identical sign increases. Figure 6(b) presents the mixing efficiency against mixing time and shows that the $\zeta_w = +150$ mV case has the longest total mixing time on account of the reduction in the flow rate through the channel. Conversely, the case with a heterogeneous surface potential of $\zeta_w = -150$ mV has the shortest total mixing time due to the increased flow rate through the channel. Compared with the uniform channel, the mixing efficiency at the channel outlet is improved by 38 and 59% for $\zeta_w = +100$ mV and $\zeta_w = +150$ mV, respectively. The corresponding mixing time is prolonged by 44 and 65% as shown in Fig. 6(b). It is evident

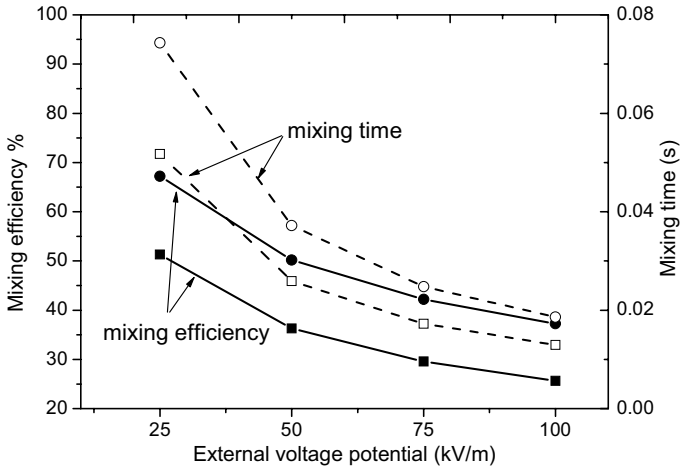

Fig. 7. Mixing efficiency and mixing time for the heterogeneous channel (circles) and uniform channel (squares) at various external voltage potentials.

that the prolonged mixing time plays a significant role in the increase in mixing efficiency.

Figure 7 presents the mixing efficiency and mixing time for the heterogeneous channel compared with the uniform channel by varying external voltage potentials. The mixing efficiency decreases as the external voltage increases due to the reduced mixing time in the microchannel. In addition, we can see that when the external voltage increases from 25 to 100 kV/m, the mixing time difference between the heterogeneous case and the uniform case decreases obviously, however, the difference in mixing efficiency between heterogeneous case and the uniform case only changes slightly, which denotes that the enhancement of heterogeneous surface is more effective when the flow velocity is larger at a higher external voltage potential.

4. Conclusions

Motivated by the growing interest in electroosmosis as a no-moving-component method to pump, mix, and control fluid motion in microfluidic devices, we have studied the common mixing enhancement method by distributing heterogeneous zeta potential on microchannel surface in EOF. We have applied a general lattice Boltzmann equation, which recovers the nonlinear Poisson–Boltzmann equation, to solve the electric potential distribution in the electrolytes, recovers the Navier–Stokes equation including the external force term, to solve the velocity field, and recovers the species convection-diffusion equation, to solve the species concentration.

We have shown that the distribution of heterogeneous zeta potential on microchannel surface can change the flow pattern by pushing the local fluid away from the heterogeneous surface region and enhance the degree of mixing. However,

the observed enhancement in the mixing efficiency is partly due to the increased total mixing time. The disturbance effect is limited by the low fluid velocity. The mixing enhancement is more efficiency when the flow velocity becomes larger. The present study recommends that the mixing time should be taken into account as well as the mixing efficient when evaluating the mixing performance of the mixing enhancing methods and it would be necessary to find a balance between them.

Acknowledgments

This work was supported by the National Natural Science Foundation of China (Grant No. 50776067) and the Program for NCET in university (Grant No. NCET-07-0676). G.H.T. would also like to express his gratitude to Yonghao Zhang in University of Strathclyde, Xiaojun Gu, Robert W. Barber, David R. Emerson in Daresbury Laboratory, STFC, UK for their helpful discussion and suggestions.

References

1. A. Ajdari, *Phys. Rev. Lett.* **75**, 755 (1995).
2. D. N. Wang, J. Summers and P. H. Gaskell, *Nanoscale Microscale Thermophys. Eng.* **11**, 1 (2007).
3. C. A. Keely, T. A. A. M. van de Goor and D. McManigil, *Anal. Chem.* **66**, 4236 (1994).
4. A. E. Herr, J. I. Molho, J. G. Santiago, M. G. Mungal, T. W. Kenny and M. G. Garguilo, *Anal. Chem.* **72**, 1053 (2000).
5. L. Q. Ren and D. Q. Li, *J. Colloid Interface Sci.* **243**, 255 (2001).
6. S. Z. Qian and H. H. Bau, *Anal. Chem.* **74**, 3616 (2002).
7. D. Erickson and D. Q. Li, *Langmuir* **18**, 1883 (2002).
8. L. M. Fu, J. Y. Lin and R. J. Yang, *J. Colloid Interface Sci.* **258**, 266 (2003).
9. F. Z. Tian, B. M. Li and D. Y. Kwok, *Langmuir* **21**, 1126 (2005).
10. B. M. Li and D. Y. Kwok, *Langmuir* **19**, 3041 (2003).
11. F. Z. Tian and D. Y. Kwok, *Langmuir* **21**, 2192 (2005).
12. J. K. Wang, M. Wang and Z. X. Li, *J. Colloid Interface Sci.* **296**, 729 (2006).
13. S. Melchionna and S. Succi, *J. Chem. Phys.* **120**, 4492 (2004).
14. Z. L. Guo, T. S. Zhao and Y. Shi, *J. Chem. Phys.* **122**, 144907 (2005).
15. Z. H. Chai, Z. L. Guo and B. C. Shi, *J. Appl. Phys.* **101**, 104913 (2007).
16. X. Y. He and L. S. Luo, *Phys. Rev. E* **56**, 6811 (1997).
17. N. A. Patankar and H. H. Hu, *Anal. Chem.* **70**, 1870 (1998).
18. J. Santiago, *Anal. Chem.* **73**, 2353 (2001).
19. L. Q. Ren and D. Q. Li, *Anal. Chim. Acta* **531**, 15 (2005).
20. Y. H. Qian, D. d'Humieres and P. Lallemand, *Europhys. Lett.* **17**, 479 (1992).
21. X. Y. He and N. Li, *Comput. Phys. Commun.* **129**, 158 (2000).
22. G. H. Tang, W. Q. Tao and Y. L. He, *Phys. Rev. E* **72**, 016703 (2005).
23. Q. Zou and X. Y. He, *Phys. Fluids* **9**, 1591 (1997).
24. P. Dutta, PhD thesis, Texas A&M University, College Station (2001).
25. R. J. Hunter, *Zeta Potential in Colloid Science* (Academic Press, London, 1981).